Mecánica Computacional Vol. XXI, pp. 183–202
S. R. Idelsohn, V. E. Sonzogni and A. Cardona (Eds.)
Santa Fe–Paraná, Argentina, October 2002

SIMULATION OF FLUID-STRUCTURE INTERACTION USING THE FEM

Paulo Roberto de F. Teixeira [*], **Armando Miguel Awruch** [†]

[*] Department of Materials and Construction, Federal University of Rio Grande - FURG
96203-000 - Rio Grande, RS, Brazil
e-mail: teixeira@dmc.furg.br

[†] Graduate Program in Civil Engineering, Applied and Computational Mechanics Center, Federal University of Rio Grande do Sul
90035-190 – Porto Alegre, RS, Brazil
e-mail: awruch@adufrgs.ufrgs.br

Key words: Fluid-structure interaction (FSI), Computational Fluid Dynamics (CFD), Geometrically non linear structural dynamics, Arbitrary Lagrangean-Eulerian (ALE) formulation

Abstract. *An algorithm to simulate 3-D fluid-structure interaction problems using the finite element technique is presented in this work. A two-step Taylor-Galerkin scheme and linear tetrahedra elements are employed to analyze the fluid flow, which may be compressible or incompressible. An Arbitrary Lagrangean-Eulerian (ALE) formulation is adopted, which must be compatible with the motion of the fluid-structure interface. A fractional method with velocity correction is used for incompressible fluids. The structure is analyzed using triangular elements with three nodes and six degrees of freedom in each node (three displacement components and three rotation components). Geometrically non-linear effects are included. The Newmark method is employed to integrate in time the dynamic equilibrium equations using an Updated Lagrangean description. The algebraic system of equations is solved using the conjugated gradient method and an incremental-iterative scheme is used to solve the non-linear system resulting from finite displacements and rotations. The code is optimized to take advantages of vector processors.*

1 INTRODUCTION

Important progress has been obtained in the solution of complex fluid-structure interaction problems in recent years, allowing the study of multidisciplinary applications in different engineering areas. This progress is due mainly to the increase of the speed of modern computers, to the evolution of multidisciplinary solution algorithms and of pre and pos-processing tools. The methods of simulation of fluid-structure interaction problems are divided basically in two groups called partitioned and monolithic schemes [1,2]. In the partitioned schemes the governing equations of the fluid and the structure are integrated in time alternately in an isolated way. In the monolithic schemes the two fields are considered as a single entity, allowing to integrate in time the two sub-domains simultaneously. In partitioned schemes such as proposed by Soria and Casadei [3], Rifai *et al.* [4], Farhat *et al.* [5], Cebral and Löhner [6] and many other authors, the kinematic and dynamic boundary conditions in the interface are the unique information changed between the sub-domains. In these schemes each sub-domain can be solved by discretization techniques and by efficient solution algorithms in an individual way. New methods and models can be introduced in a modular way in order to get more flexibility. Besides, the meshes of each sub-domain can be built without the coincidence of fluid and structural nodes at the interfaces [6,7]. These modular characteristics and flexibility may be extremely convenient.

An algorithm to simulate fluid-structure interaction problems using a partitioned scheme is presented in this work. A two-step explicit Taylor-Galerkin scheme [8,9], with linear tetrahedral finite elements is employed. An Arbitrary Lagrangean-Eulerian (ALE) description is adopted for the fluid domain, while for the structural domain an Updated Lagrangean formulation is considered. The structure is analyzed using generalized conforming triangular plates and shell elements with drilling degrees of freedom [10]. Geometrically non linear effects are included. The Newmark method [11] is employed to integrate in time the dynamic equilibrium equation. The non linear and the algebraic systems are solved using an incremental-iterative scheme and the conjugate gradient method, respectively. The code was vectorized to take advantages of vectorial processors. Two problems are used to validate the methods developed in this work and illustrate the difference between linear and non linear aeroelastic computations.

2 THE FLUID DYNAMIC SOLVER

2.1 The explicit two-step Taylor-Galerkin scheme for compressible flows

In the ALE description, the computational frame is a reference independent of the particle movement and may be moving with an arbitrary velocity in the laboratory system (this motion is called the "mesh" motion in the finite element formulation); the continuum view from this reference is denoted as Ω_χ and the coordinates of any point are denoted as χ [12]. The equations expressing mass, momentum and energy conservation in ALE formulation may be written in a compact form as

$$\left.\frac{\partial \mathbf{V}}{\partial t}\right|_{\chi} + \frac{\partial \mathbf{F}_i}{\partial x_i} = w_i \frac{\partial \mathbf{V}}{\partial x_i} \qquad (i=1,2,3) \tag{1}$$

with $\mathbf{F}_i = \mathbf{F}_{iA} + \mathbf{F}_{iD}$ and

$$\mathbf{V} = \begin{Bmatrix} \rho \\ \rho \mathrm{v}_1 \\ \rho \mathrm{v}_2 \\ \rho \mathrm{v}_3 \\ \rho \varepsilon \end{Bmatrix}; \quad \mathbf{F}_{iA} = \begin{Bmatrix} \rho \mathrm{v}_i \\ \rho \mathrm{v}_1 \mathrm{v}_i + p\,\delta_{i1} \\ \rho \mathrm{v}_2 \mathrm{v}_i + p\,\delta_{i2} \\ \rho \mathrm{v}_3 \mathrm{v}_i + p\,\delta_{i3} \\ \mathrm{v}_i(\rho\varepsilon + p) \end{Bmatrix}; \; \mathbf{F}_{iD} = \begin{Bmatrix} 0 \\ -\tau_{1i} \\ -\tau_{2i} \\ -\tau_{3i} \\ -\tau_{ij}\,\mathrm{v}_j - k_{ij}\,\partial T / \partial x_j \end{Bmatrix} \quad (i,j=1,2,3) \tag{2}$$

where v_i and w_i are the fluid and the mesh velocity components in the direction of the spatial coordinate x_i respectively, ρ is the density, p is the thermodynamic pressure, τ_{ij} are the components of the deviatoric stress tensor, T is the temperature, ε is the total specific energy and k_{ij} are the components of the conductivity tensor; vector $\mathbf{V}$ contains the conservation or the field variables and $\mathbf{F}_i$ are the components of the flux variables ($\mathbf{F}_{iA}$ contains the advective terms and $\mathbf{F}_{iD}$ the viscous terms). Finally, δ_{ij} is the Kronecker delta. Equation (1) is complemented by the equation of state for an ideal gas and by the constitutive equations. Initial and boundary conditions must be added to these equations in order to define uniquely the problem.

In the Taylor-Galerkin scheme, conservation equations are expanded in time by Taylor series, and after, space discretization is accomplished by the classical Bubnov-Galerkin scheme. A two-step method is used [8] in which can be interpreted as the finite element version of the Lax-Wendroff scheme used in finite differences [13]. In the first step, corresponding to the time interval $[t^n, t^{n+1/2}]$, the unknown vector $\mathbf{V}$ at $t=t^{n+1/2}$ is expanded in Taylor series. Using a linear shape function $\mathbf{N}$ associated with each node to interpolate $\mathbf{V}^n$, a constant shape function $\mathbf{P}_E=1$ associated with element E to interpolate $\mathbf{V}^{n+1/2}$ and applying the classical Galerkin weighted residual method to the expression resulting from Taylor series expansion, the following equation is obtained:

$$\begin{aligned} \Omega_E^{n+1/2}\,\mathbf{V}_E^{n+1/2} &= \left(\int_{\Omega_E^n} \mathbf{N} \; d\Omega \right) \overline{\mathbf{V}}^n \\ -\frac{\Delta t}{2} &\left[\left(\int_{\Omega_E^n} \frac{\partial \mathbf{N}}{\partial x_i} \, d\Omega \right) \overline{\mathbf{F}}_i^n - \left(\int_{\Omega_E^n} \mathbf{N} \; \overline{\mathbf{w}}_i^n \frac{\partial \mathbf{N}}{\partial x_i} \, d\Omega \right) \overline{\mathbf{V}}^n \right] \quad (i=1,2,3) \end{aligned} \tag{3}$$

where $\Omega_E^{n+1/2}$ is the element volume, $\mathbf{V}_E^{n+1/2}$ is a constant value at element level and the upper bar indicates nodal variables.

In the second step, the unknown vector at $t=t^{n+1}$ is expanded in Taylor series. Using again the same shape functions, and applying the Bubnov-Galerkin method, the following equation is obtained for the second step:

$$\left(\int_{\Omega_E^{n+1}} \mathbf{N}^T \mathbf{N}\, d\Omega\right)\overline{\mathbf{V}}^{n+1} = \left(\int_{\Omega_E^{n}} \mathbf{N}^T \mathbf{N}\, d\Omega\right)\overline{\mathbf{V}}^{n} + \Delta t\left(\int_{\Omega_E^{n+1/2}} \frac{\partial \mathbf{N}}{\partial x_i}\, d\Omega\right)\left(\overline{\mathbf{F}}_i^{n+1/2} - \overline{\mathbf{w}}_i^{n+1/2}\overline{\mathbf{V}}^{n+1/2}\right)$$
$$- \Delta t\left(\int_{\Gamma_E^{n+1/2}} \mathbf{N}\, l_i\, d\Gamma\right)\left(\overline{\mathbf{F}}_{Bi}^{n+1/2} - \overline{\mathbf{w}}_{Bi}^{n+1/2}\overline{\mathbf{V}}_B^{n+1/2}\right) \quad (i=1,2,3) \tag{4}$$

where $\Gamma_E^{n+1/2}$ is the boundary of the element domain $\Omega_E^{n+1/2}$ and l_i is the cosine of the angle formed by the outward normal axis to $\Gamma_E^{n+1/2}$ with the positive direction of the reference axis x_i. Index B is referred to values at the boundary of the element domain. In Eq. (4), the consistent mass matrix is substituted by the lumped mass matrix, and then this equation is solved iteratively. The proposed scheme is conditionally stable, and the local stability condition is applied.

In order to stabilize numerically the solution, specially in the presence of strong shocks, it is necessary to add numerical damping to the flow solver. In this work the viscosity model [14], is adopted. An artificial viscosity is added explicitly to the non-smoothed solution, as follows

$$\overline{\mathbf{V}}_s^{n+1} = \overline{\mathbf{V}}^{n+1} + \left(\mathbf{M}_L^{n+1}\right)^{-1}\mathbf{D} \tag{5}$$

where $\overline{\mathbf{V}}_s^{n+1}$ and $\overline{\mathbf{V}}^{n+1}$ are the smoothed and non-smoothed solution at $t=t^{n+1}$, respectively. $\mathbf{M}_L^{n+1}$ is the assembled lumped mass matrix at $t=t^{n+1}$. The vector $\mathbf{D}$ is given by

$$\mathbf{D} = \sum\nolimits_E CFL_E\, CC\, \overline{S}_E \left[\mathbf{M}_{EC}^n - \mathbf{M}_{EL}^n\right]\overline{\mathbf{V}}_E^n, \tag{6}$$

where E is an index referred to a specific element, CFL_E is the local Courant number, CC is a global constant specified by the user, $\overline{S}_E$ is a coefficient of pressure distribution [8,9], $\mathbf{M}_{EC}^n$ and $\mathbf{M}_{EL}^n$ are the consistent and lumped mass matrices, respectively.

2.2 The two-step Taylor-Galerkin scheme for incompressible flows

Mass conservation for slightly compressible fluids, assuming constant entropy, may be expressed by the following equation:

$$\frac{\partial \rho}{\partial t} = \frac{1}{c^2}\frac{\partial p}{\partial t} = -\frac{\partial U_i}{\partial x_i} \quad (i=1,2,3), \tag{7}$$

where c is the sound speed and $U_i = \rho\, \mathrm{v}_i$ $(i=1,2,3)$.

Expanding the momentum conservation equations in Taylor series, the following expression is obtained for the first step:

$$U_i^{n+1/2} = U_i^n + \frac{\Delta t}{2}\frac{\partial U_i^n}{\partial t} = U_i^n - \frac{\Delta t}{2}\left(\frac{\partial f_{ij}^n}{\partial x_j} - \frac{\partial \tau_{ij}^n}{\partial x_j} + \frac{\partial p^n}{\partial x_i} + \frac{1}{2}\frac{\partial \Delta p}{\partial x_i} - w_j^n\frac{\partial U_i^n}{\partial x_i}\right) (i,j=1,2,3), \tag{8}$$

where $f_{ij} = \mathrm{v}_j U_i$ (i,j=1,2,3) and $p^{n+1/2} = p^n + 1/2\,\Delta p$, with $\Delta p = p^{n+1} - p^n$. Using

$$\widetilde{U}_i^{n+1/2} = U_i^n - \frac{\Delta t}{2}\left(\frac{\partial f_{ij}^n}{\partial x_j} - \frac{\partial \tau_{ij}^n}{\partial x_j} + \frac{\partial p^n}{\partial x_i} - w_j^n \frac{\partial U_i^n}{\partial x_i}\right) \quad (i,j=1,2,3)\,, \tag{9}$$

Eq. (8) is given by the following expression:

$$U_i^{n+1/2} = \widetilde{U}_i^{n+1/2} - \frac{\Delta t}{4}\frac{\partial \Delta p}{\partial x_i} \quad (i=1,2,3)\,. \tag{10}$$

Discretizing Eq. (7) in time and using Eq. (10), it is obtained:

$$\Delta\rho = \frac{1}{c^2}\Delta p = -\Delta t \frac{\partial U_i^{n+1/2}}{\partial x_i} = -\Delta t\left[\frac{\partial \widetilde{U}_i^{n+1/2}}{\partial x_i} - \frac{\Delta t}{4}\frac{\partial}{\partial x_i}\frac{\partial \Delta p}{\partial x_i}\right] \quad (i = 1,2,3)\,. \tag{11}$$

The second time step is given by the following expression:

$$U_i^{n+1} = U_i^n + \Delta t \frac{\partial U_i^{n+1/2}}{\partial t} = U_i^n - \Delta t\left(\frac{\partial f_{ij}^{n+1/2}}{\partial x_j} - \frac{\partial \tau_{ij}^{n+1/2}}{\partial x_j} + \frac{\partial p^{n+1/2}}{\partial x_i} - w_j^{n+1/2}\frac{\partial U_i^{n+1/2}}{\partial x_i}\right) (i,j=1,2,3) \tag{12}$$

Then the flow is analyzed, after space discretization, by the following algorithm: (1) determine $\widetilde{U}_i^{n+1/2}$ with Eq. (9); (2) determine Δp with Eq. (11) and calculate $p^{n+1} = p^n + \Delta p$; (3) determine $U_i^{n+1/2}$ with Eq. (10); (4) determine U_i^{n+1} with Eq. (12).

Considering the same shape functions used in compressible flows and applying the classical Galerkin method for space discretization, the following matrix expressions are obtained for Eq. (9), (11), (10) and (12), respectively:

$$\begin{aligned}\Omega_E^{n+1/2}\widetilde{\mathbf{U}}_{iE}^{n+1/2} = \left(\int_{\Omega^n}\mathbf{N}\;d\Omega\right)\overline{\mathbf{U}}_i^n - \frac{\Delta t}{2}\Bigg[\left(\int_{\Omega^n}\frac{\partial \mathbf{N}}{\partial x_j}d\Omega\right)\overline{\mathbf{f}}_{ij}^n - \left(\int_{\Omega^n}\frac{\partial \mathbf{N}}{\partial x_j}d\Omega\right)\overline{\tau}_{ij}^n \\ + \left(\int_{\Omega^n}\frac{\partial \mathbf{N}}{\partial x_i}d\Omega\right)\overline{\mathbf{p}}^n - \left(\int_{\Omega^n}\mathbf{N}\,\overline{\mathbf{w}}_j^n\frac{\partial \mathbf{N}}{\partial x_j}d\Omega\right)\overline{\mathbf{U}}_i^n\Bigg] \quad (i,j=1,2,3)\end{aligned} \tag{13}$$

$$\begin{aligned}\left(\int_{\Omega^{n+1/2}}\mathbf{N}^T\frac{1}{c^2}\mathbf{N}\;d\Omega + \frac{\Delta t^2}{4}\int_{\Omega^{n+1/2}}\frac{\partial \mathbf{N}^T}{\partial x_i}\frac{\partial \mathbf{N}}{\partial x_i}\;d\Omega\right)\Delta\overline{\mathbf{p}} = \Delta t\Bigg[\left(\int_{\Omega^{n+1/2}}\frac{\partial \mathbf{N}^T}{\partial x_i}\;d\Omega\right)\widetilde{\mathbf{U}}_{iE}^{n+1/2} \\ -\left(\int_{\Gamma^{n+1/2}}\mathbf{N}^T\mathbf{n}_i\,d\Gamma\right)\widetilde{\mathbf{U}}_{iE}^{n+1/2}\Bigg] \quad (i=1,2,3)\end{aligned} \tag{14}$$

$$\Omega_E^{n+1/2}\ \ \mathbf{U}_{iE}^{n+1/2} = \Omega_E^{n+1/2}\ \ \widetilde{\mathbf{U}}_{iE}^{n+1/2} - \frac{\Delta t}{4}\left(\int_{\Omega^{n+1/2}} \frac{\partial \mathbf{N}}{\partial x_i}\ d\Omega\right) \Delta\overline{\mathbf{p}} \qquad (i=1,2,3) \tag{15}$$

$$\begin{aligned}
&\left(\int_{\Omega^{n+1}} \mathbf{N}^T \mathbf{N}\, d\Omega\right)\ \overline{\mathbf{U}}_i^{n+1} = \left(\int_{\Omega^n} \mathbf{N}^T \mathbf{N}\, d\Omega\right)\ \overline{\mathbf{U}}_i^{n} + \Delta t\left(\int_{\Omega^{n+1/2}} \frac{\partial \mathbf{N}^T}{\partial x_j}\ d\Omega\right)\ \left(\mathbf{f}_{ij}^{n+1/2} - \mathbf{w}_j^{n+1/2}\mathbf{U}_i^{n+1/2}\right)_E \\
&\quad - \Delta t\left(\int_{\Omega^{n+1/2}} \frac{\partial \mathbf{N}^T}{\partial x_j}\mathbf{N}\ \ d\Omega\right)\ \overline{\tau}_{ij}^{n} + \Delta t\left(\int_{\Omega^{n+1/2}} \frac{\partial \mathbf{N}^T}{\partial x_i}\mathbf{N}\ \ d\Omega\right)\left(\overline{\mathbf{p}}^n + \Delta\overline{\mathbf{p}}/2\right) \\
&\quad - \Delta t\left(\int_{\Gamma^{n+1/2}} \mathbf{N}^T \mathbf{n}_j\, d\Gamma\right)\left(\mathbf{f}_{ij}^{n+1/2} - \mathbf{w}_j^{n+1/2}\mathbf{U}_i^{n+1/2}\right)_E \\
&+ \Delta t\left(\int_{\Gamma^{n+1/2}} \mathbf{N}^T \mathbf{N}\ \ \mathbf{n}_j\, d\Gamma\right)\ \overline{\tau}_{ij}^{n} - \Delta t\left(\int_{\Gamma^{n+1/2}} \mathbf{N}^T \mathbf{N}\ \ \mathbf{n}_i\, d\Gamma\right)\left(\overline{\mathbf{p}}^n + \Delta\overline{\mathbf{p}}/2\right) \quad (i,j=1,2,3)
\end{aligned} \tag{16}$$

In Eq. (13) to (16) the index *E* indicates that the corresponding variables are taken with a constant value over the element domain. Eq. (14) is solved using the conjugate gradient method with diagonal pre conditioning.

2.3 The algorithm for mesh movement

The mesh velocity field **w** is computed looking for small element distortions, conserving prescribed velocities in moving and stationary boundary surfaces. The mesh movement algorithm adopted in this work uses a smoothing procedure for the velocities based in these boundary surfaces. The updating of the mesh velocity at a point *i* of the finite element domain is based on the mesh velocity of the points *j* belonging to the boundary surfaces in the following way (see Fig. 1):

$$\mathbf{w}^i = \frac{\sum_{j=1}^{ns} a_{ij}\, \mathbf{w}^j}{\sum_{j=1}^{ns} a_{ij}} \tag{17}$$

where *ns* is the total number of points belonging to the boundary surfaces and a_{ij} are the influence coefficients between the point *i* inside the domain and the point *j* of the boundary surface given by the following expression:

$$a_{ij} = \frac{1}{d_{ij}^4} \tag{18}$$

with d_{ij} being the distance between the points i and j. In other words, a_{ij} represents the weight that each point j of the boundary surface has on the value of the mesh velocity at points i inside the domain. When d_{ij} is small, a_{ij} has an high value, favouring the influence of points i, located closer to the boundary surface containing point j.

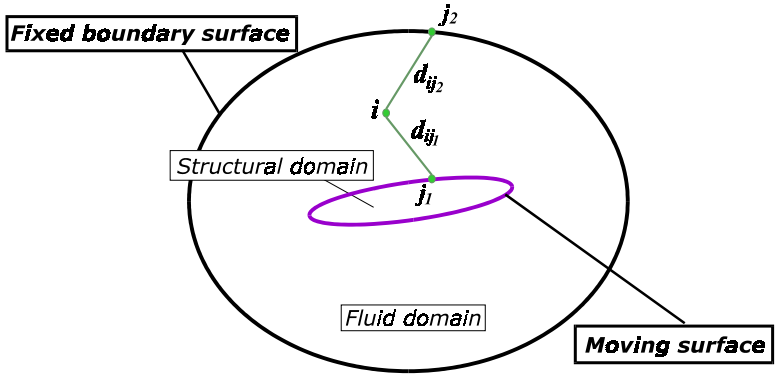

Figure 1: Distances from the boundary surfaces to a point "*i*" in the fluid domain

3 THE STRUCTURAL DYNAMIC SOLVER WITH A TRIANGULAR THIN PLATE ELEMENT

A generalized conforming triangular thin plate element including the drilling degree of freedom, in which the compatibility conditions at each node and along each side are applied, is used in the present work (see Fig. 2) [10].

The total stiffness matrix of the element is obtained by the overlap of the membrane stiffness matrix with the bending stiffness matrix. A typical membrane triangular element is adopted where each point has two degrees of freedom of translation u_{xi} and u_{yi} (i = 1,2,3) and one of rotation θ_{zi} (i = 1,2,3) in the plane of the element middle surface. The membrane displacements are expressed in the following way:

$$\mathbf{u}_m = \begin{bmatrix} u_x & u_y \end{bmatrix}^T = \mathbf{N}_m \mathbf{u}_m^e \tag{19}$$

where $\mathbf{u}_m^e$ is the nodal membrane generalized displacements vector given by

$$\mathbf{u}_{mi}^e = \begin{bmatrix} u_{xi} & u_{yi} & \theta_{zi} \end{bmatrix}^T \quad (i=1,2,3) \tag{20}$$

and $\mathbf{N}_m$ is the membrane interpolation function defined as follows:

$$\mathbf{N}_{mi} = \begin{bmatrix} L_i & 0 & N_{u\theta i} \\ 0 & L_i & N_{v\theta i} \end{bmatrix} \quad (i=1,2,3) \tag{21}$$

being L_i the area coordinates and

$$N_{u\theta i} = \frac{1}{2} L_i \left(b_m L_j - b_j L_m \right), \quad N_{v\theta i} = \frac{1}{2} L_i \left(c_m L_j - c_j L_m \right), \quad b_i = y_j - y_m \ , \quad c_i = x_m - x_j \quad (i,j,m=1,2,3) \tag{22}$$

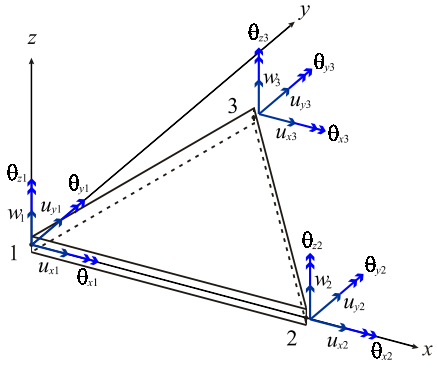

Figure 2: The thin plate triangular element

The transverse displacement field is discretized by

$$u_z = \mathbf{N}_b \, \mathbf{u}_b^e \tag{23}$$

where $\mathbf{u}_b^e$ is the nodal bending generalized displacements vector, which is written in the following way:

$$\mathbf{u}_{bi}^e = \left[u_{zi} \quad \theta_{xi} \quad \theta_{yi} \right]^T \quad (i=1,2,3) \tag{24}$$

being u_{zi} the nodal transverse displacements, and θ_{xi} and θ_{yi} the nodal rotations around the axes x and y, respectively. $\mathbf{N}_b$ is the bending interpolation function given by

$$N_{bi} = \left[N_i \quad N_{xi} \quad N_{yi} \right]^T \quad (i=1,2,3) \tag{25}$$

with

$$N_i = L_i - 2F_i + (1 - r_j) F_j + (1 + r_m) F_m$$

$$N_{xi} = -\frac{1}{2} \left[b_m L_i L_j - b_j L_m L_i + (b_j - b_m) F_i + (r_j b_j + b_m) F_j + (r_m b_m - b_j) F_m \right]$$

$$N_{yi} = -\frac{1}{2} \left[c_m L_i L_j - c_j L_m L_i + (c_j - c_m) F_i + (r_j c_j + c_m) F_j + (r_m c_m - c_j) F_m \right] \tag{26}$$

$$F_i = L_i\left(L_i - 0.5\right)\left(L_i - 1\right), \quad r_i = \frac{1}{l_{jm}^2}\left(l_{im}^2 - l_{ij}^2\right), \quad l_{ij} = \sqrt{x_{ij}^2 + y_{ij}^2},$$

$$x_{ij} = x_i - x_j, \quad y_{ij} = y_i - y_j \quad (i,j,m=1,2,3)$$

The linear stiffness matrix at element level due to membrane and bending effects are given, respectively, by the following expressions:

$$\mathbf{K}_{Lmi} = \int_{\Omega^{(e)}} \mathbf{B}_{mi}^T \mathbf{D}_m \mathbf{B}_{mi} \, d\Omega \; ; \quad \mathbf{K}_{Lbi} = \int_{\Omega^{(e)}} \mathbf{B}_{bi}^T \mathbf{D}_b \mathbf{B}_{bi} \, d\Omega \quad (i=1,2,3) \tag{27}$$

where $\Omega^{(e)}$ is the element domain. The constitutive matrices $\mathbf{D}_m$ and $\mathbf{D}_b$ are given, respectively, by

$$\mathbf{D}_m = \frac{Eh}{1-\nu^2}\mathbf{D}; \qquad \mathbf{D}_b = \frac{E\,h^3}{12\left(1-\nu^2\right)}\mathbf{D}; \qquad \mathbf{D} = \begin{bmatrix} 1 & \nu & 0 \\ \nu & 1 & 0 \\ 0 & 0 & (1-\nu)/2 \end{bmatrix} \tag{28}$$

where h is the elements thickness, ν the Poisson's ratio and E the Young's modulus. Finally, the strain-displacement relations are

$$\mathbf{B}_{mi} = \frac{1}{4\,\Omega^{(e)}} \begin{bmatrix} 2b_i & 0 & b_i\left(b_m L_j - b_j L_m\right) \\ 0 & 2c_i & c_i\left(c_m L_j - c_j L_m\right) \\ 2c_i & 2b_i & \left(c_i b_m + b_i c_m\right)L_j - \left(c_i b_j + b_i c_j\right)L_m \end{bmatrix} \quad (i,j,m=1,2,3) \tag{29}$$

and

$$\mathbf{B}_{bi} = -\begin{bmatrix} N_{i,xx} & N_{xi,xx} & N_{yi,xx} \\ N_{i,yy} & N_{xi,yy} & N_{yi,yy} \\ 2N_{i,xy} & 2N_{xi,xy} & 2N_{yi,xy} \end{bmatrix} \quad (i=1,2,3) \tag{30}$$

The non linear geometric stiffness matrix is given by

$$\mathbf{K}_{NLi} = \int_{\Omega^{(e)}} \mathbf{G}_{Gi}^T \, \mathbf{T}_i \mathbf{G}_{Gi} \, d\Omega \quad (i=1,2,3) \tag{31}$$

where $\mathbf{T}_i$ contains the membrane internal forces and is given by

$$\mathbf{T}_i = \begin{bmatrix} \mathbf{T}_{xxi} & \mathbf{T}_{xyi} \\ \mathbf{T}_{yxi} & \mathbf{T}_{yyi} \end{bmatrix} \quad (i=1,2,3) \tag{32}$$

with

$$\mathbf{T}_{xxi} = \left[\sum_{k=1}^{3} \mathbf{D}_m(1,k).\mathbf{B}_{mi}(k,1)\right].\mathbf{u}_{mi}(1)$$

$$\mathbf{T}_{yyi} = \left[\sum_{k=1}^{3} \mathbf{D}_m(2,k).\mathbf{B}_{mi}(k,2)\right].\mathbf{u}_{mi}(2) \tag{33}$$

$$\mathbf{T}_{xyi} = \left[\sum_{k=1}^{3} \mathbf{D}_m(3,k).\mathbf{B}_{mi}(k,3)\right].\mathbf{u}_{mi}(1) = \mathbf{T}_{yxi} \quad (i=1,2,3)$$

while $\mathbf{G}_{Gi}$ is given by

$$\mathbf{G}_{Gi} = \begin{bmatrix} N_{i,x} & N_{xi,x} & N_{yi,x} \\ N_{i,y} & N_{xi,y} & N_{yi,y} \end{bmatrix} \quad (i=1,2,3) \tag{34}$$

The dynamic equilibrium equations of the structural system are obtained by the space discretization of the virtual work equations, which must be solved for each time step using a numerical integration scheme. In the present work the well-known Newmark method is used[11], with parameters $\delta = 1/2$ and $\alpha = 1/4$. In geometrically non linear problems the solution of these balance equations is accomplished for each time step with an incremental iterative procedure using an Updated Lagrangean formulation. The resulting system of algebraic equations are solved using the gradient conjugate method with incomplete Cholesky factorization.

4 THE FLUID-STRUCTURE INTERACTION ALGORITHM

Commonly, fluid and structure fields have different scales of time. The global time step is usually commanded by the fluid. Although the use of the same time step for the fluid and the structure may provide some implementation advantages, the procedure with subcycles of factor $n_{SF} = \Delta t_S / \Delta t_F$ (where Δt_S and Δt_F are the time intervals adopted for the structure and the fluid, respectively) may offer substantial computational advantages, including an economy of CPU time due to the smaller number of time steps in the structural analysis and an economy in the information transfer. The partitioned algorithm with subcycles adopted in the present work consists in the following steps (see Fig. 3):

(a) Set the initial conditions for the structure and the fluid.
(b) Update the structure displacements, velocities, accelerations and stresses.
(c) Update the fluid velocities, specific mass, pressure and total energy using subcycles.
  (c.1) Compute the new mesh taken into account the structural motion.
  (c.2) Update the fluid flow variables with the new boundary conditions.
(d) Update the structural variables with the loads transferred by the fluid.
(e) Repeat steps (c) and (d) until the objectives of the simulation are reached.

Kinematics boundary conditions, taken into account the structural motion, must be applied to the fluid domain. Therefore, at the fluid-structure interface the following condition must be satisfied:

$$x_i^{n+1}\big|_{\Gamma_F} = {}^{t+\Delta t}x_i\big|_{\Gamma_E} \quad (i=1,2,3)\,, \tag{35}$$

where $x_i^{n+1}\big|_{\Gamma_F}$ and ${}^{t+\Delta t}x_i\big|_{\Gamma_E}$ are the updated coordinates for the instant $t+\Delta t$ at the fluid and solid interfaces Γ_F and Γ_E, respectively. For viscous fluids the same velocity components are prescribed for the mesh, the fluid and the structure at the interface. Therefore,

$$\mathrm{w}_i^{n+1}\big|_{\Gamma_F} = \mathrm{v}_i^{n+1}\big|_{\Gamma_F} = {}^{t+\Delta t}\dot{u}_i\big|_{\Gamma_E} \quad (i=1,2,3). \tag{36}$$

For non viscous fluids the corresponding prescribed boundary conditions are:

$$\mathrm{w}_i^{n+1}\big|_{\Gamma_F}\cdot n_i = \mathrm{v}_i^{n+1}\big|_{\Gamma_F}\cdot n_i = {}^{t+\Delta t}\dot{u}_i\big|_{\Gamma_E}\cdot n_i \quad (i=1,2,3)\,, \tag{37}$$

where n_i is the normal versor with respect to the interface surface at time $t+\Delta t$. Equation (37) is applied to each node located in the interface surface.

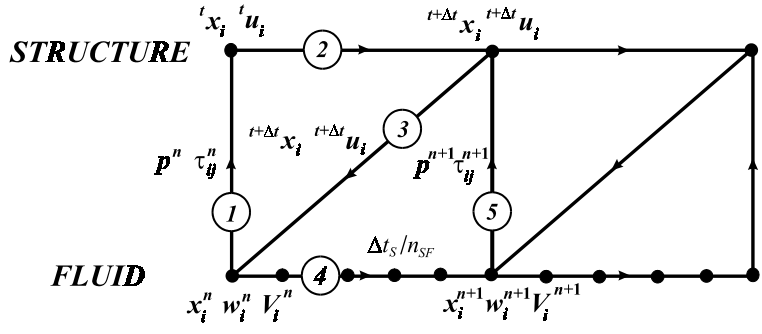

Figure 3: Algorithm for fluid-structure interaction with subcycles

5 NUMERICAL APPLICATIONS

5.1 Unsteady flow around an oscillating NACA0012 airfoil

In this example an inviscid transonic flow (Mach number M=0.755) over the NACA0012 airfoil, with a rotational vibration around a point located at the quarter chord, is analized. The movement of the airfoil is prescribed such that the angle of attack varies according to the following relation:

$$\alpha = \alpha_m + \alpha_0 \,\mathrm{sen}\,(2\,M_\infty\, k\,\bar{t}\,)\,, \tag{38}$$

where $\alpha_m = 0.016\ deg$ is the mean angle of attack, $\alpha_0 = 2.51\ deg$ is the unsteady angle of attack amplitude, $\bar{t}$ is the dimensionless time and the chord length L_a is used as the reference length. The NACA0012 airfoil is assumed to rotate with a reduced frequency $k = 0.0814$, defined as $k = w_a L_a / 2 v_\infty$, where w_a is the frequency in radians per second and v_∞ is the freestream velocity.

Boundary conditions in the planes of symmetry *xy* and in the other external surfaces are prescribed. Boundary conditions given by Eq. (35) and (37) are prescribed in the fluid-structure interface. A non structured mesh with 5150 nodes and 21700 tetrahedral elements, with only one layer of elements in the perpendicular direction to the flow, is used for the fluid domain and is shown in Fig.4.

The unsteady calculations start from a steady-state solution. $CC = 2.0$ and $\Delta t = 0.00025$ are adopted for the damping constant of Eq. (6) and for the smallest dimensionless time interval, respectively. A multi-time-step integration technique [9] is used, resulting in a theoretical computational saving of 2.38.

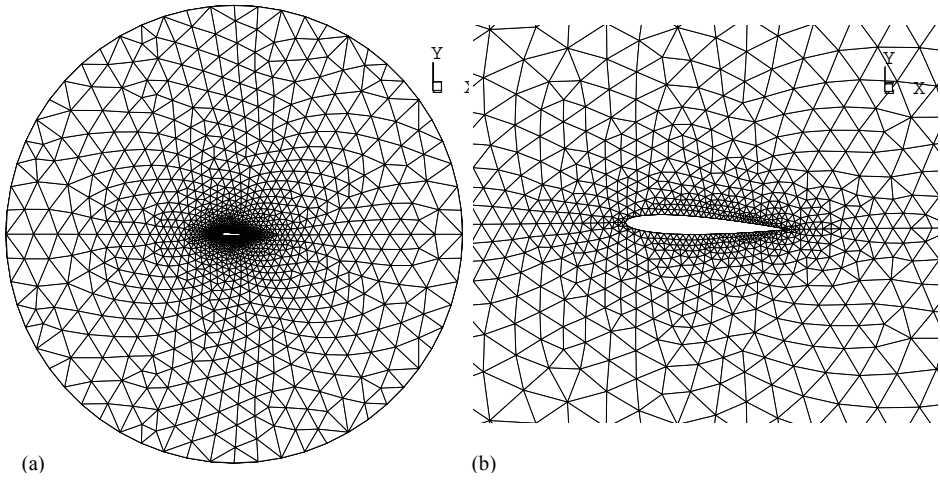

Figure 4: Finite element mesh. (a) General view. (b) Detail of the region close to the airfoil

Fig. 5 shows the lift coefficient C_L plotted against the time-dependent angle of attack α and time per period $w_a t/2\pi$. A comparison with the experimental results [15] and obtained by Crumpton and Giles [16] and Willcox and Peraire [17] is presented in this figure. Pressure distributions are shown in Fig. 6 for $t = 12.544$ ($\alpha = 2.525^o$) and $t = 40.768$ ($\alpha = -2.383^o$).

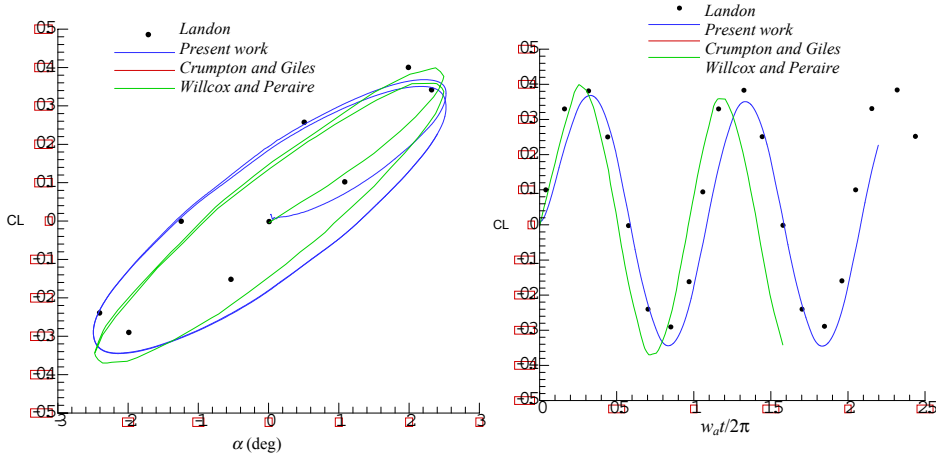

Figure 5: Lift coefficient C_L as function of angle of attack α and time per period $w_a t/2\pi$

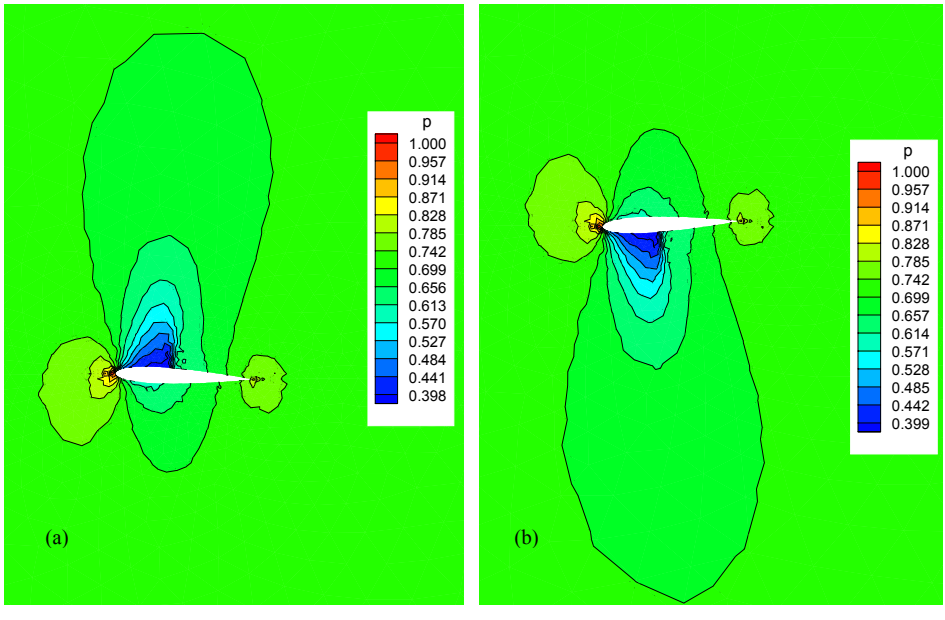

Figure 6: Distribution of pressure for (a) $t = 12.544$ ($\alpha = 2.525^o$) and (b) $t = 40.768$ ($\alpha = -2.383^o$)

5.2 Air flow past an inflated membrane

The interaction between air flow (considered as an incompressible flow) and a flexible membrane is analyzed. The problem is described in Fig. 7. The membrane has a semi-cylindrical format with diameter d and width h equal to 20 m and 3.0 mm, respectively, and is clamped at both ends.

The external boundary of the fluid domain is a semi-cylinder with radius R and width L in the perpendicular direction to the plane where the flow takes place equal to 200 m and 1 m, respectively. At the external boundary a velocity profile, which is a function of the distance with respect to the ground level, is prescribed. This velocity is referred to the velocity at 10 m above the ground level, which varies with time. This function is smoothed at $t = 0\ s$, $3\ s$, $6\ s$ and $9\ s$ using a quadratic senoidal function. A reference pressure p=0 is prescribed in the point located in the external boundary condition, 200 m above the ground level. The air and membrane properties are given in Tab. 1. The internal pressure p_o, which keeps the membrane inflated, is taken equal to 60% of the air stagnation pressure at a velocity of 28 m/s ($p_o = 285.0$ Pa).

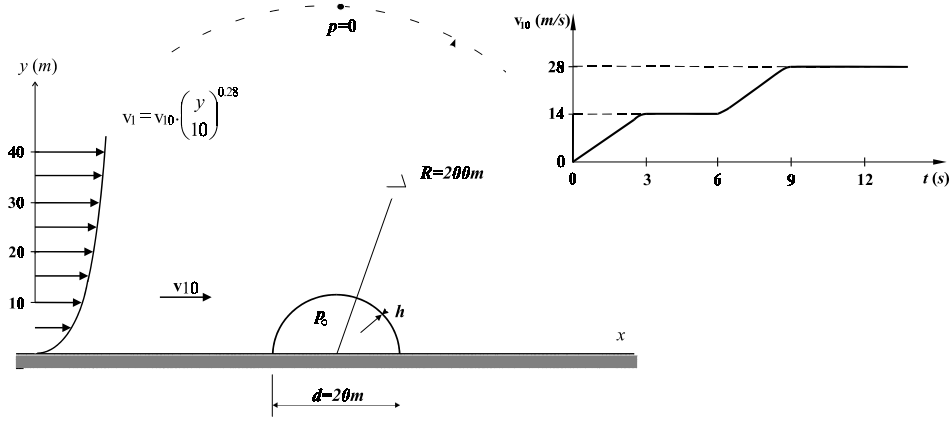

Figure 7: Description of the problem to study the interaction between air flow and a flexible membrane

Table 1: Air and membrane properties

Membrane properties	Value
Young's modulus E	3.333×10^8 N/m^2
Poisson's ratio ν	0.0
Specific mass ρ_E	1000.0 Kg/m^3

Air properties	Value
Sound speed C_∞	345 m/s
Kinematic viscosity μ	17.9×10^{-6} Pa.s
Specific mass ρ_F	1.21 Kg/m^3

Due to the existence of air inside the space covered by the membrane, a damping matrix is included to analyze the structure. A Rayleigh viscous damping is adopted, which means that

$$\mathbf{C} = \alpha\mathbf{M} + \beta\mathbf{K} \tag{39}$$

where **C**, **M** and **K** are the damping, mass and stiffness matrices, respectively. Considering a linear behaviour, adopting damping ratios equal to $\xi_1 = 1.0\%$ e $\xi_2 = 2.0\%$ for the first and second modes, respectively, and calculating the corresponding circular frequencies ω_1 and ω_2, the coefficient α and β can be determined by the procedure described in Bathe [11]. For this case, $\alpha = 0.003529$ and $\beta = 0.443162$ are obtained.

Although this case is essentially a two-dimensional problem and beam elements for the structure may be used, a three-dimensional code is employed, where the membrane model was built with triangular flat elements and the fluid domain was discretized with tetrahedral elements. In the perpendicular direction to the flow, only one layer of elements is used.

The non structured finite element mesh in the fluid domain has 20550 tetrahedral elements and 7097 nodes, as indicated in Fig. 8. The structural mesh has 124 nodes and 124 triangular elements (these elements are coincident with the faces of the tetrahedral elements at the fluid-structure interface). The prescribed boundary conditions on the lateral ends are $w=\theta_x=\theta_y=0$ for the plate and $v_3=0$ for the fluid domain.

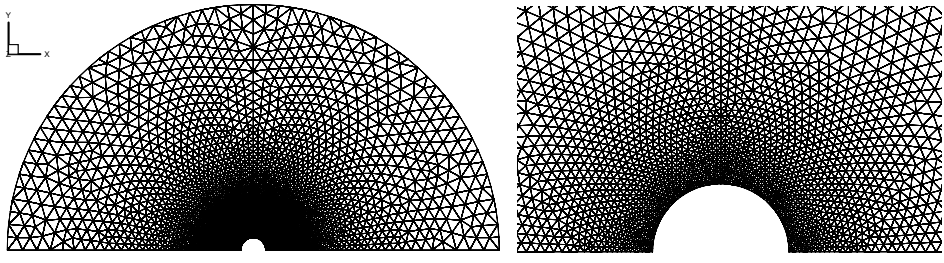

(a) (b)

Figure 8: Finite element mesh. (a) General view. (b) Detail of the region close to the membrane

As Reynolds number in this problem is relatively high if it is determined with a reference velocity equal to 28 m/s and a reference length equal to the radius of the structure (10 m) a simple algebraic turbulence model is used. This model was also employed by Mittal and Tezduyar [18], and consists in the addition of a eddy viscosity μ_T to the molecular kinematic viscosity μ. The eddy viscosity is given by the following expression

$$\mu_T = (Kl)^2 \sqrt{\frac{1}{2}\left(\frac{\partial v_i}{\partial x_j} + \frac{\partial v_j}{\partial x_i}\right) : \left(\frac{\partial v_i}{\partial x_j} + \frac{\partial v_j}{\partial x_i}\right)}, \tag{40}$$

where $K = 0.41$ is the Von Kármán constant and l is the shortest distance between the point where μ_T will be determined and the closest wall to this point.

A dimensionless time interval Δt_F=1.25x10^{-3}.is adopted for the fluid domain, while a time step Δt_S=1.25x10^{-4} is used to analyze the membrane. Pressure distributions, velocity vectors and mesh configurations in the fluid domain are shown in Fig. 9, Fig 10 and Fig. 11, respectively for t = 1.5 *s*, 3.0 *s*, 6.0 *s*, 9.0 *s*, 10.5 *s* e 12.0 *s*.

Membrane configurations obtained in the present work are very similar to those presented by Argyris[19]. However, pressure distributions and velocity vectors here show that downstream recirculating flows occur along time. This phenomenon was not well captured by the above mentioned reference, probably because the finite element mesh was poorly refined (taking into account the characteristics of this problem).

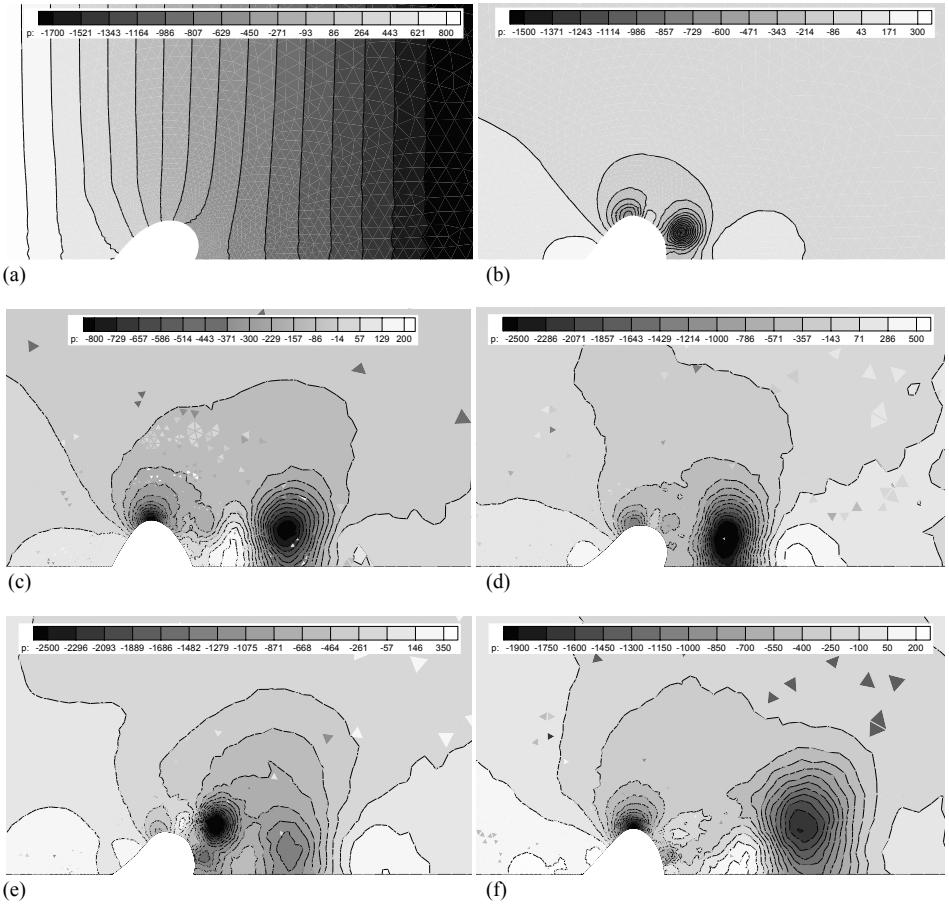

Figure 9: Pressure distribution at the instants (a) 1.5 *s*, (b) 3.0 *s*, (c) 6.0 *s*, (d) 9.0 *s*, (e) 10.5 *s* and (f) 12.0 *s*

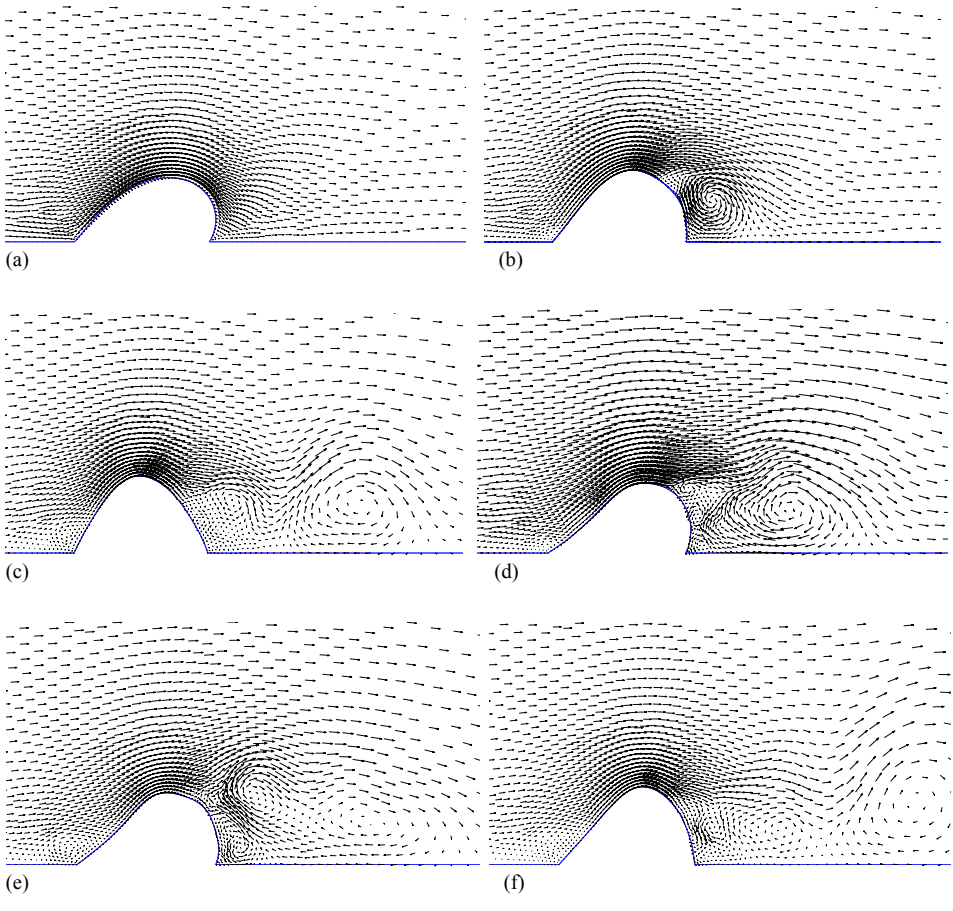

Figure 10: Velocity vectors at the instants (a) 1.5 s, (b) 3.0 s, (c) 6.0 s, (d) 9.0 s, (e) 10.5 s and (f) 12.0 s

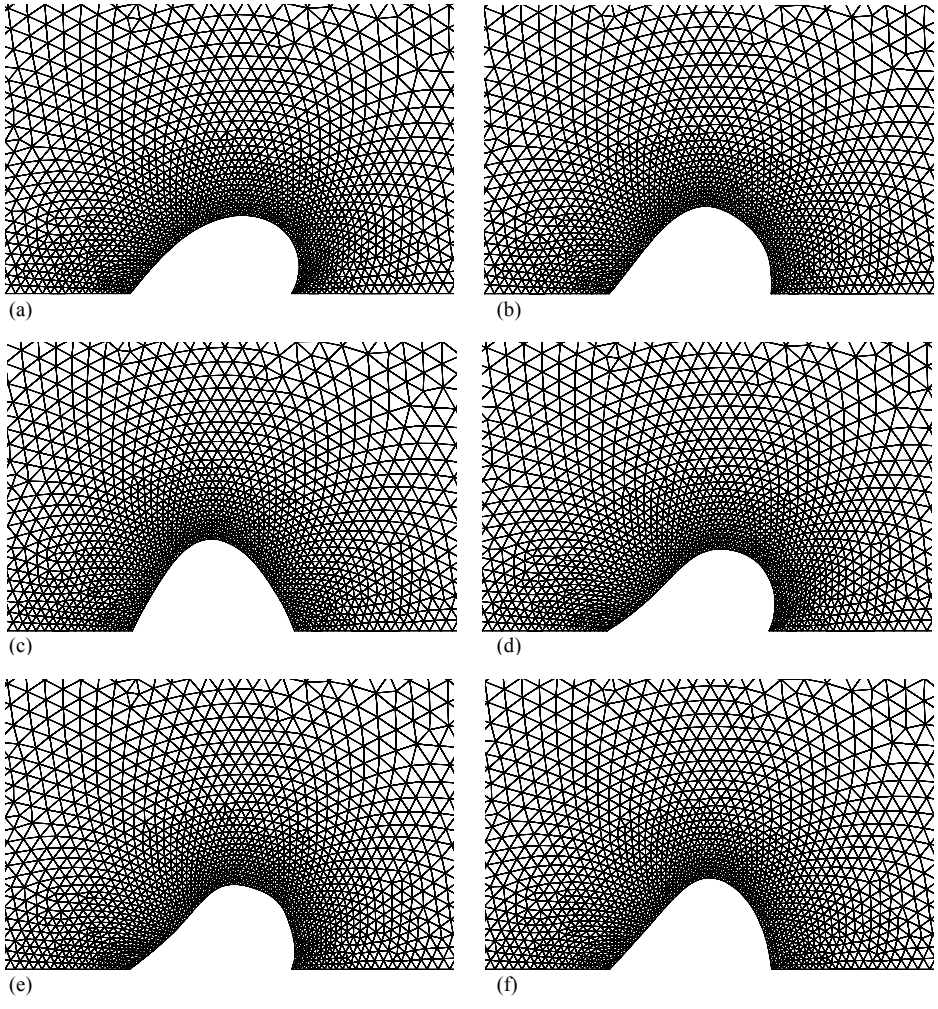

Figure.11: Mesh configurations in the fluid domain at (a) 1.5 *s*, (b) 3.0 *s*, (c) 6.0 *s*, (d) 9.0 *s*, (e) 10.5 *s* and (f) 12.0 *s*

6. CONCLUSIONS

A partitioned algorithm for the solution of fluid-structure interaction problems using a two-step Taylor-Galerkin method for the fluid in the ALE formulation and the Newmark implicit scheme for the solution of the structural dynamic equations is presented in this work.

The capability of the method was shown solving examples with incompressible and compressible flows, where satisfactory results were obtained. The good performance of the vectorized algorithms was verified. Speeds going from 670 to 888 Mflops in a Cray T94 computer and with a CPU time of the order of 1.2 to 2.3×10^{-5} $s/\Delta t$ *node* have been obtained.

Acknowledgement

The authors wish to thank CNPq and CAPES for the financial support.

7. REFERENCES

[1] F.F. Felker, "Direct solution of two-dimensional Navier-Stokes equations for static aeroelasticity problems", AIAA Journal, **31**(1), 148-153 (1993).

[2] F.J. Blom, "A monolithical fluid-structure interaction algorithm applied to the piston problem", Computer Methods in Applied Mechanics Engineering, **167**, 369-391 (1998).

[3] A. Soria and F. Casadei, "Arbitrary Lagrangian-Eulerian multicomponent compressible flow with fluid-structure interaction", International Journal for Numerical Methods in Fluids, **25**, 1263-1284 (1997).

[4] S.M. Rifai *et al*., "Multiphysics simulation of flow-induced vibrations and aeroelasticity on parallel computing platforms", Computer Methods in Applied Mechanics Engineering, **174**, 393-417 (1999).

[5] C. Farhat, M. Lesoinne and N. Maman, "Mixed explicit/implicit time integration of coupled aeroelastic problems: three-field formulation, geometric conservation and distributed solution", International Journal for Numerical Methods in Fluids, **21**, 807-835 (1995).

[6] J.R. Cebral and R. Löhner, "Conservative load projection and tracking for fluid-structure problems", AIAA Journal, **35**, 687-692 (1997).

[7] C. Farhat, M. Lesoinne and P. LeTallec, "Load and motion transfer algorithms for fluid/structure interaction problems with non-matching discrete interfaces: momentum and energy conservation, optimal discretization and application to aeroelasticity", Computer Methods in Applied Mechanics Engineering, **157**, 95-114 (1998).

[8] O.C. Zienkiewicz, R. Lönher, K.O. Morgan and J. Peraire, "High speed compressible flow and other advection-dominated problems of fluid dynamics", Finite Elements in Fluids (Ed. By R. Gallagher *et al*.), **6**, 41-48 (1988).

[9] P.R.F. Teixeira and A.M. Awruch, "Three-dimensional simulation of high compressible flows using a multi-time-step integration technique with subcycles", Applied Mathematical Modelling, **25**/7, 613-627 (2001).

[10] Q. Zhang, L. Um and K. Wenqi, "Geometric non-linear analysis of space shell structures using generalized conforming flat shell elements – for space shell structures", Communications in Numerical Methods in Engineering, **14**, 941-957 (1998).

[11] K. Bathe, *Finite element procedures*, Prentice Hall, Englewood Cliffs, NJ, USA, (1996).
[12] W.K. Liu, H. Chang, J.S. Chen and T. Belytschko, "Arbitrary Lagrangean-Eulerian Petrov-Galerkin finite elements for non linear continua", Computer Methods in Applied Mechanics Engineering, **68**, 259-310 (1988).
[13] R.D. Richtmeyer and K.W. Morton, *Difference methods for initial value problems*, Interscience, New York, (1967).
[14] J. Peraire *et al*., "Finite element Euler computations in three dimensions", International Journal for Numerical Methods in Engineering, **26**, 2135-2159 (1988).
[15] R.H. Landon "NACA0012 oscilatory and transient pitching", AGARD R-702 (1982).
[16] P.I. Crumpton and M.B. Giles "Implicit time – accurate solutions on unstructured dynamic grids", International Journal Numerical Methods in Fluids, **25**, 1285-1300 (1997).
[17] K. Willcox and J. Peraire "Aeroelastic computations in the time domain using unstrucutred meshes", International Journal for Numerical Methods in Engineering, **40**, 2413-2431 (1997).
[18] S. Mittal and T.E. Tezduyar "Parallel finite element simulation of 3D incompressible flows: fluid-structure interactions", International Journal for Numerical Methods in Fluids, **21**, 933-953 (1995).
[19] J. ARGYRIS *et al*. "Τα παντα ρει", Computer Methods in Applied Mechanics and Engineering, **51**, 289-362 (1985).